Endoscopic forward-viewing optical coherence tomography and angiography with MHz swept source

Citation: Liang, Kaicheng et al. "Endoscopic forward-viewing optical coherence tomography and angiography with MHz swept source." Optics Letters 42, 16 (August 2017): 3193-3196 © 2017 Optical Society of America

As Published: http://dx.doi.org/10.1364/ol.42.003193

Publisher: Optical Society of America

Persistent URL: https://hdl.handle.net/1721.1/121580

Version: Author's final manuscript: final author's manuscript post peer review, without publisher's formatting or copy editing

HHS Public Access

Author manuscript

Opt Lett. Author manuscript; available in PMC 2018 March 29.

Published in final edited form as:

Opt Lett. 2017 August 15; 42(16): 3193–3196.

Endoscopic forward-viewing optical coherence tomography and angiography with MHz swept source

Kaicheng Liang[1,iD], **Osman O. Ahsen**[1], **Zhao Wang**[1], **Hsiang-Chieh Lee**[1], **Wenxuan Liang**[2], **Benjamin M. Potsaid**[1,3], **Tsung-Han Tsai**[1], **Michael G. Giacomelli**[1], **Vijaysekhar Jayaraman**[4], **Hiroshi Mashimo**[5,6], **Xingde Li**[2], and **James G. Fujimoto**[1,*]

[1]Department of Electrical Engineering and Computer Science, and Research Laboratory of Electronics, Massachusetts Institute of Technology, Cambridge, Massachusetts 02139, USA

[2]Department of Biomedical Engineering, Johns Hopkins University, Baltimore, Maryland 21218, USA

[3]Thorlabs, Newton, New Jersey 07860, USA

[4]Praevium Research, Santa Barbara, California 93111, USA

[5]Veterans Affairs Boston Healthcare System, Boston, Massachusetts 02130, USA

[6]Harvard Medical School, Boston, Massachusetts 02115, USA

Abstract

Endoscopic optical coherence tomography (OCT) instruments are mostly side viewing and rely on at least one proximal scan, thus limiting accuracy of volumetric imaging and *en face* visualization. Previous forward-viewing OCT devices had limited axial scan speeds. We report a forward-viewing fiber scanning 3D-OCT probe with 900 μm field of view and 5 μm transverse resolution, imaging at 1 MHz axial scan rate in the human gastrointestinal tract. The probe is 3.3 mm diameter and 20 mm rigid length, thus enabling passage through the endoscopic channel. The scanner has 1.8 kHz resonant frequency, and each volumetric acquisition takes 0.17 s with 2 volumes/s display. 3D-OCT and angiography imaging of the colon was performed during surveillance colonoscopy.

Endoscopic optical coherence tomography (OCT) using minimally invasive catheters is an emerging imaging modality in gastroenterology [1,2]. Early studies demonstrated side-viewing catheters that scanned the OCT beam by proximal rotary and pullback actuation of a torque cable [3]. This design has enabled imaging of luminal organs and continues to be the workhorse of commercially available catheter OCT systems [1]. Proximal actuation via a long catheter with multiple bends produces nonuniform rotational and/or longitudinal distortion [4,5]. Recent catheters have used distal rotary scanning micromotors, reducing rotational distortion [6–8]. Our group developed new methods for side-viewing OCT that use distal actuation for 2D scanning [9]. Distal scanning enables OCT angiography (OCTA), which uses repeated scans to detect motion contrast from blood flow to visualize

*Corresponding author: jgfuji@mit.edu.

Kaicheng Liang https://orcid.org/0000-0003-3237-4034

microvasculature and has been used extensively in ophthalmology [10]. Our group recently demonstrated endoscopic OCTA using distal micromotor scanning [6,11].

Forward-viewing OCT catheters are of clinical interest because they generate images analogous to endoscopic views [12] and can examine small regions of interest (ROIs) at high resolution. Forward-viewing devices using microelectromechanical systems (MEMS) [13] or piezoelectric actuators [14,15] enable distal 2D scanning and are thus immune to catheter bending. These devices exploit mechanical resonances for scanning and are uniquely suited for high-speed OCT due to their high scan speed [16,17].

We report a forward-viewing OCT piezoelectric probe and endoscopic imaging in the human gastrointestinal (GI) tract *in vivo*. The probe has a 3.3 mm diameter and 20 mm rigid length and can be used in the endoscopic accessory channel, thus enabling use in existing endoscopic workflows. Volumetric OCT and OCTA were performed at a 1 MHz axial scan (A-scan) rate to image colonic mucosa and a hyperplastic polyp in human patients. The high-speed laser was a critically enabling factor in clinical translation of OCT/OCTA, particularly in endoscopy, where patient motion is significant, and rapid volumetric display with adequate image sampling is essential. The ability to perform high A-scan speed endoscopic forward-viewing OCT has clinical potential for providing volumetric and *en face* microscopic tissue assessment.

The OCT system [6] [Fig. 1(A)] used a dual circulator interferometer with a MEMS vertical cavity surface emitting laser (VCSEL) swept source at 1310 nm (Thorlabs/Praevium) [18] running at ~500 kHz sweep rate, producing a ~1 MHz bidirectional A-scan rate. The exact VCSEL repetition rate was set to a high integer multiple of the probe resonant frequency, and the waveform generator used to drive the VCSEL also was used to clock the D/A board, simplifying electronic synchronization. The OCT interferometer and detector sensitivity was 103 dB at an incident power of 35 mW on the sample. The probe one-way transmission was 80%; therefore, the effective system sensitivity was ~100 dB. Losses were due to imperfect circulators/couplers, use of fiber mating sleeves instead of splices, and imperfect optical surfaces of the probe lens and fiber cleave. The imaging range was 2.1 mm in air, and the axial resolution was 9 μm in tissue. The A/D board (AlazarTech 9370) was optically clocked up to 1.1 GHz by a Mach–Zehnder interferometer. Optical clocking with linear in k sampling enabled direct Fourier transformation, thus simplifying post-processing. A D/A board (National Instruments PCIe-6323) generated amplitude-modulated sinusoidal waveforms to drive a piezoelectric actuator, which were synchronized to the start of each volumetric acquisition. The phase-shifted sinusoidal waveforms produced a spiral [Fig. 2(B)] fiber scanning trajectory.

The resonant fiber scanning probe [Figs. 1(B) and 1(C)] was similar to previous devices [14,15,19]. An optical fiber was mounted to the tip of a piezoelectric (lead zirconate titanate) tube (Boston Piezo-Optics, Bellingham, Massachusetts) of 6 mm length, 1.5 mm outer diameter, 0.3 mm wall, and quartered electrodes for two-axis actuation. A <20 mm rigid length of the probe was necessary for passage through the 3.7 mm endoscopic accessory channel; therefore, the piezoelectric actuator length was minimized, costing a reduction in actuating range. The fiber was aligned to a 1.8 mm diameter gradient index lens (Go!Foton,

Somerset, New Jersey) for 1:1 magnification to the focal plane (~200 μm deep in tissue contacting with lens). The piezoelectric actuator, optical fiber, and lens were housed in a 12G hypotube. The entire device was encapsulated in American Wire Gauge 9 fluorinated ethylene propylene tubing, with no exposed conductive surfaces, and sealed watertight using medical epoxy.

The piezoelectric actuator was driven by waveforms from a four-channel current limited 50× amplifier. The output voltage after amplification was 40 V peak amplitude A.C., within the recommended limit from the International Electrotechnical Commission medical electrical apparatus standards [20]. Electrodes on the actuator were precision laser etched (Laser Impressions, Sunnyvale, California) for symmetric actuation. It also was important for the fiber mount to be centered and symmetric in the tube, so that resonance frequency and amplitude would be similar in both axes. The fiber was centered in the tube with a ring jewel bearing (Swiss Jewel, Philadelphia, Pennsylvania) and fixed with heat-cured epoxy for optimal rigidity, ensuring a high (> 100) resonant quality (Q) factor. The resonating fiber deflection was measured using a consumer webcam CCD sensor fitted with a microscope objective.

The scanner resonance was determined by fiber length, estimated using the fixed-free cantilever formula [19]. The fiber length was 7.5 mm, producing a theoretical resonant frequency of ~1800 Hz on the fast circular scan. The fiber scanned at ~900 μm diameter, which was equal to the field of view (FOV) at 1:1 magnification. The 9 μm mode field diameter ($1/e^2$) of SMF-28 gave 5 μm FWHM transverse resolution and ~600 resolvable spots on the outermost circle. At 1 MHz A-scan rate, each resonant period had ~600 A-scans, such that the outermost circle was sampled at half-Nyquist (5 μm pitch). Each volume had 300 circular scans; the FOV radius was ~450 μm (~90 resolvable spots); therefore, the slow radial axis was sampled at 3× Nyquist. For OCTA, volumes were acquired at half the scan field (~450 μm diameter), such that the outermost circle was Nyquist sampled, and the slow axis sampled at 6× Nyquist.

After probe assembly was completed, the fiber was scanned in a spiral, and the trajectory assessed using a position-sensitive detector (PSD, On-Trak, Irvine, California). The phase difference and amplitudes of the two axes driving the fiber were tuned for optimal circularity [15]. The trajectory measured by the PSD was recorded and used to generate a nearest-neighbor look-up table (LUT) for converting the spiral to a 512 × 512 Cartesian grid. The trajectory was stable regardless of probe orientation, and re-calibration was required after one to two weeks. Each volume was acquired in 0.17 s and processed by the acquisition software (C++) for *en face* display before the next acquisition. The volume was acquired with the fiber actuated with increasing amplitude (outward spiral) because an inward spiral did not accurately follow the drive waveform phase. The repeat volume rate was limited by time required for the fiber to damp naturally, an additional ~0.2 s. Processing introduced a further delay resulting in ~2 volumes/s rate. Processing of spectral data was performed in MATLAB. Each OCT volume was remapped to the spiral using the LUT. Cross-sectional images analogous to traditional B-scans were extracted from the remapped volumes. OCT angiograms were post-processed and calculated by intensity decorrelation [6,21] of the raw circular scans, which did not require registration. Remapping was performed after

decorrelation. OCT volumes were used to generate OCTA; therefore, the OCT and OCTA images were intrinsically co-registered at all depths.

Imaging was performed at the Veterans Affairs Boston Healthcare System (VABHS) with approvals at the Massachusetts Institute of Technology, VABHS, and Harvard Medical School, and written informed consent obtained. Inclusion criteria was colonoscopy. The probe was introduced into the accessory channel and placed in gentle contact with ROIs in the endoscopic view to minimize compression. Multiple volumes were acquired at each location to overcome potential imaging artifacts from bulk motion.

The fiber scanner had a measured resonance of 1762 Hz [Fig. 2(A)]. The resonance peak frequency for either axis was the same; however, the amplitude for one axis was lower at the same driving voltage. This might be related to asymmetry in fiber mounting or etching of actuator electrodes. It was possible to reduce amplitude on one axis to improve circularity; however, it was preferable to optimize FOV. Figure 2(C) shows a test image of a nylon grid placed on top of an absorbent fiber pad, just before the endoscopy. The probe was held by hand and placed in contact with the grid. The image had stable reconstruction of the grid, with minor distortions due to the non-telecentricity of the field. The resolution was sufficient to visualize the absorbent fibers that were tens of micrometers thick.

Imaging was performed on normal colonic mucosa (Fig. 3). Cross-sectional OCT images showed vertically projecting features associated with colonic crypts. The *en face* plane at shallower depth showed circular/elliptical crypts and structural features reminiscent of crypt lumens. At deeper depths, OCT showed integrated effects of light propagation/backscattering; crypt walls produced high OCT signal, while lumens and stroma produced dark vertical features, resulting in contrast inversion [8]. Imaging of a benign hyperplastic polyp (Fig. 4) showed regular crypts but slightly enlarged and more sparsely distributed, in this single illustrative example. OCTA of the polyp (Fig. 5) showed vascular patterns varying with depth and encircling the crypts.

In endoscopic and minimally invasive scenarios using catheters, 2D distal actuation for scanning is attractive. The repeat volume rate in this study was limited because of the time for the fiber to damp before rescanning. A large resonant deflection was required to maximize FOV, but the high Q resonance produced a ~0.2 s damping time, limiting the volume rate. The fiber resonant motion may be actively damped by driving with a waveform of the opposite quadrature, but accurate phasing is required [15]. Graphics processing units could reduce the processing delay.

Forward-viewing devices are an important complement to side viewing. While side-viewing probes have large FOV, they are inefficient for targeting small regions flagged on the endoscopic view and requiring a closer look. Proximal scan errors exacerbate the difficulty of visualizing small regions. Forward viewing has small FOV but is suited for close-up inspection.

The resolution of scanning fiber devices depends on the number of resolvable spots, which is calculated from the fiber mode field diameter and the scan range. Constraints of the probe rigid length and driving voltages impose a limit on resolvable spots. Smaller actuators (~400

μm diameter) have been reported [15] but are not yet commercially available. Deflection is inversely proportional to tube diameter and wall thickness [22]; smaller actuators scan larger fields for a given voltage, which will increase resolvable spot numbers and relax requirements for high Q factors.

The resonant scan sampled at constant angular velocity, such that sampling decreased with increasing radial distance. While this resulted in nonuniform sampling, it enabled sequential circular scans to be decorrelated to generate OCTA because the spots were radially aligned. The fast resonance produced scan overlap, but the short (0.57 ms) interscan time reduced sensitivity to slow flows in small vessels. Constant linear velocity would produce uniform sampling but cannot easily generate OCTA. Although there was oversampling in the fast axis toward the center due to decreasing length of the circular scans, the latter increased uncertainty in scan-to-scan alignment; therefore, decorrelation noise did not necessarily decrease toward the center. Noise artifacts mimicking the spiral were likely due to small synchronization errors between the laser and scanner and small parasitic motion.

In GI endoscopy, the concept of “resect and discard,” i.e., assessing polyps to be benign *in situ* and discarding them without histopathological analysis, is gaining traction as a potentially more cost-effective surveillance protocol, given the significant cost of histology processing [23]. The polyp in this study did not exhibit marked structural anomalies on imaging and later showed benign histology. In this context, forward-viewing OCT has promise in providing real-time tissue assessment during endoscopy.

Ultrahigh-speed OCT at 1 MHz A-scan rate with a forward-viewing probe generated high-quality volumetric and *en face* images of colonic microstructure and vascularity. Future work will assess adenomas and other colonic pathology to evaluate the diagnostic potential of forward-viewing OCT in GI surveillance.

Acknowledgments

KCL acknowledges an Agency for Science, Technology and Research (Singapore) graduate fellowship.

Funding. National Institutes of Health (NIH) (F32-CA183400, R01-CA075289, R01-CA178636, R01-EY011289, R44-CA101067); Air Force Office of Scientific Research (AFOSR) (FA9550-12-1-0499, FA9550-15-1-0473).

References

1. Leggett CL, Gorospe EC, Chan DK, Muppa P, Owens V, Smyrk TC, Anderson M, Lutzke LS, Tearney G, Wang KK. Gastrointest. Endosc. 2016; 83:880. [PubMed: 26344884]
2. Aguirre, AD. Advances in Optical Coherence Tomography and Microscopy for Endoscopic Applications and Functional Neuroimaging. Massachusetts Institute of Technology; 2008.
3. Tearney GJ, Brezinski ME, Bouma BE, Boppart SA, Pitris C, Southern JF, Fujimoto JG. Science. 1997; 276:2037. [PubMed: 9197265]
4. Ahsen OO, Lee H-C, Giacomelli MG, Wang Z, Liang K, Tsai T-H, Potsaid B, Mashimo H, Fujimoto JG. Opt. Lett. 2014; 39:5973. [PubMed: 25361133]
5. Uribe-Patarroyo N, Bouma BE. Opt. Lett. 2015; 40:5518. [PubMed: 26625040]
6. Tsai T-H, Ahsen OO, Lee H-C, Liang K, Figueiredo M, Tao YK, Giacomelli MG, Potsaid BM, Jayaraman V, Huang Q, Cable AE, Fujimoto JG, Mashimo H. Gastroenterology. 2014; 147:1219. [PubMed: 25172015]
7. Jing JC, Chou L, Su E, Wong BJF, Chen Z. Sci. Rep. 2016; 6:39443. [PubMed: 27991580]

8. Liang K, Ahsen OO, Lee H-C, Wang Z, Potsaid BM, Figueiredo M, Jayaraman V, Cable AE, Huang Q, Mashimo H, Fujimoto JG. Am. J. Gastroenterol. 2016; 111:1664. [PubMed: 27808130]
9. Liang K, Traverso G, Lee H-C, Ahsen OO, Wang Z, Potsaid B, Giacomelli M, Jayaraman V, Barman R, Cable A, Mashimo H, Langer R, Fujimoto JG. Biomed. Opt. Express. 2015; 6:1146. [PubMed: 25909001]
10. Makita S, Hong Y, Yamanari M, Yatagai T, Yasuno Y. Opt. Express. 2006; 14:7821. [PubMed: 19529151]
11. Lee H-C, Ahsen OO, Liang K, Wang Z, Cleveland C, Booth L, Potsaid B, Jayaraman V, Cable AE, Mashimo H, Langer R, Traverso G, Fujimoto JG. Biomed. Opt. Express. 2016; 7:2927. [PubMed: 27570688]
12. Kudo S-E, Tamura S, Nakajima T, Yamano H-O, Kusaka H, Watanabe H. Gastrointest. Endosc. 1996; 44:8. [PubMed: 8836710]
13. Seo Y-H, Hwang K, Park H-C, Jeong K-H. Opt. Express. 2016; 24:3903. [PubMed: 26907043]
14. Huo L, Xi JF, Wu YC, Li XD. Opt. Express. 2010; 18:14375. [PubMed: 20639922]
15. Lee CM, Engelbrecht CJ, Soper TD, Helmchen F, Seibel EJ. J. Biophoton. 2010; 3:385.
16. Zhang N, Tsai T-H, Ahsen OO, Liang K, Lee H-C, Xue P, Li X, Fujimoto JG. Opt. Lett. 2014; 39:186. [PubMed: 24562102]
17. Lurie KL, Gurjarpadhye AA, Seibel EJ, Ellerbee AK. Opt. Lett. 2015; 40:3165. [PubMed: 26125393]
18. Jayaraman, V., Jiang, J., Li, H., Heim, PJS., Cole, GD., Potsaid, B., Fujimoto, JG., Cable, A. Conference on Lasers and Electro- Optics (CLEO). IEEE; 2011.
19. Liu X, Cobb MJ, Chen Y, Kimmey MB, Li X. Opt. Lett. 2004; 29:1763. [PubMed: 15352362]
20. “Medical Electrical Equipment: General Requirements for Basic Safety and Essential Performance,” IEC 60601-1:2005. International Electrotechnical Commission; 2005. p. 69-70.
21. Jonathan E, Enfield J, Leahy MJ. J. Biophoton. 2011; 4:293.
22. Chen CJ. Appl. Phys. Lett. 1992; 60:132.
23. Hassan C, Pickhardt PJ, Rex DK. Clin. Gastroenterol. Hepatol. 2010; 8:865. [PubMed: 20621680]

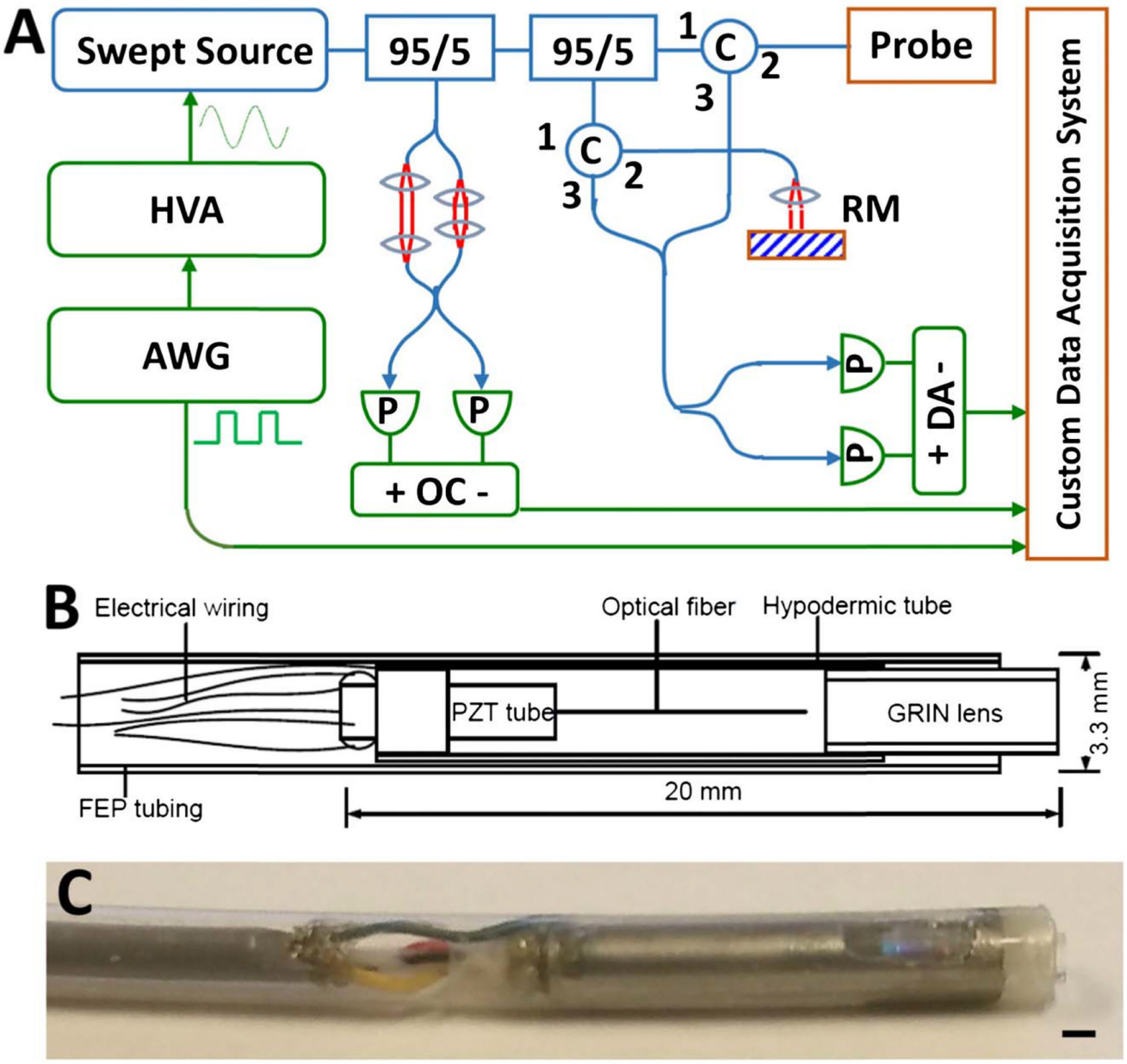

Fig. 1.

(A) Ultrahigh-speed OCT system. HVA, high-voltage amplifier; AWG, arbitrary waveform generator; P, photodetector; C, circulator; RM, reference mirror; OC, optical clock; DA, differential amplifier. (B) Schematic and (C) photo of forward-viewing probe (scale bar 1 mm).

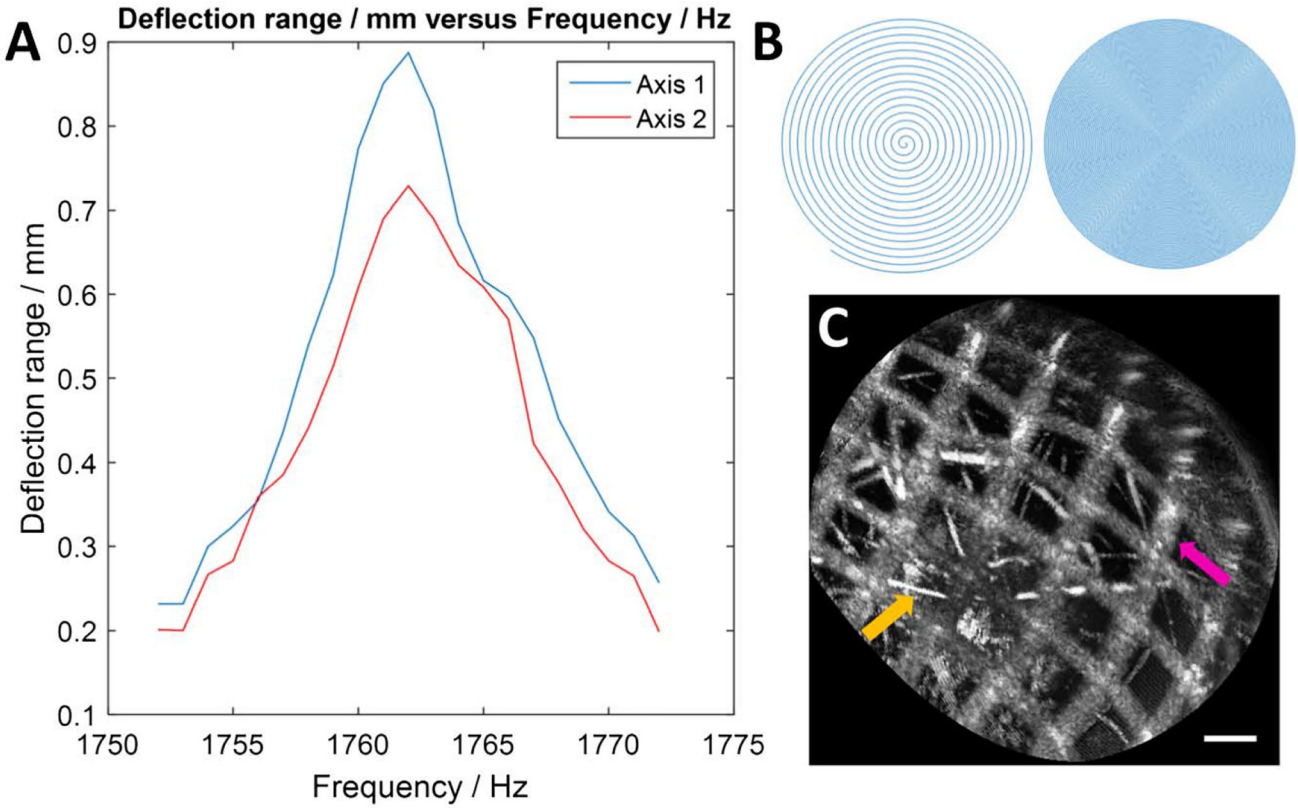

Fig. 2.

(A) Frequency response of the fiber scanner. (B) Illustration of spiral scan showing sparse/dense sampling. (C) *En face* OCT image of a nylon grid (pink arrow) of pitch 140 μm placed over an absorbent fiber pad (orange), acquired with the probe (scale bar 100 μm).

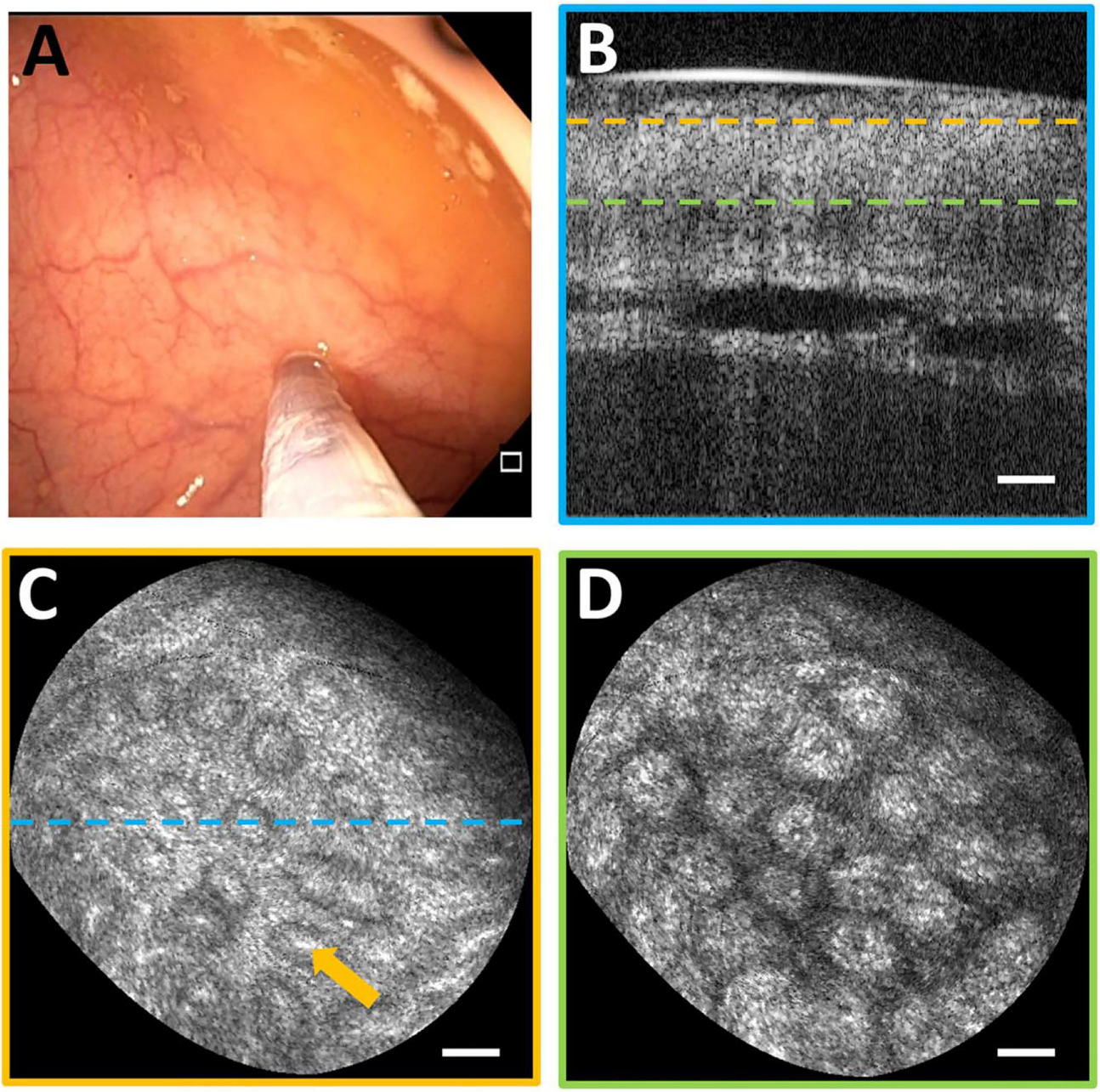

Fig. 3.

(A) Endoscopic image showing probe in contact with normal colonic mucosa. (B) Cross-section of OCT volume acquired. *En face* OCT slices of 40 μm depth mean intensity projection at (C) 40 μm depth and (D) 200 μm depth in tissue (dashed lines indicate depth) showing crypt lumens (orange arrow). Scale bars 100 μm.

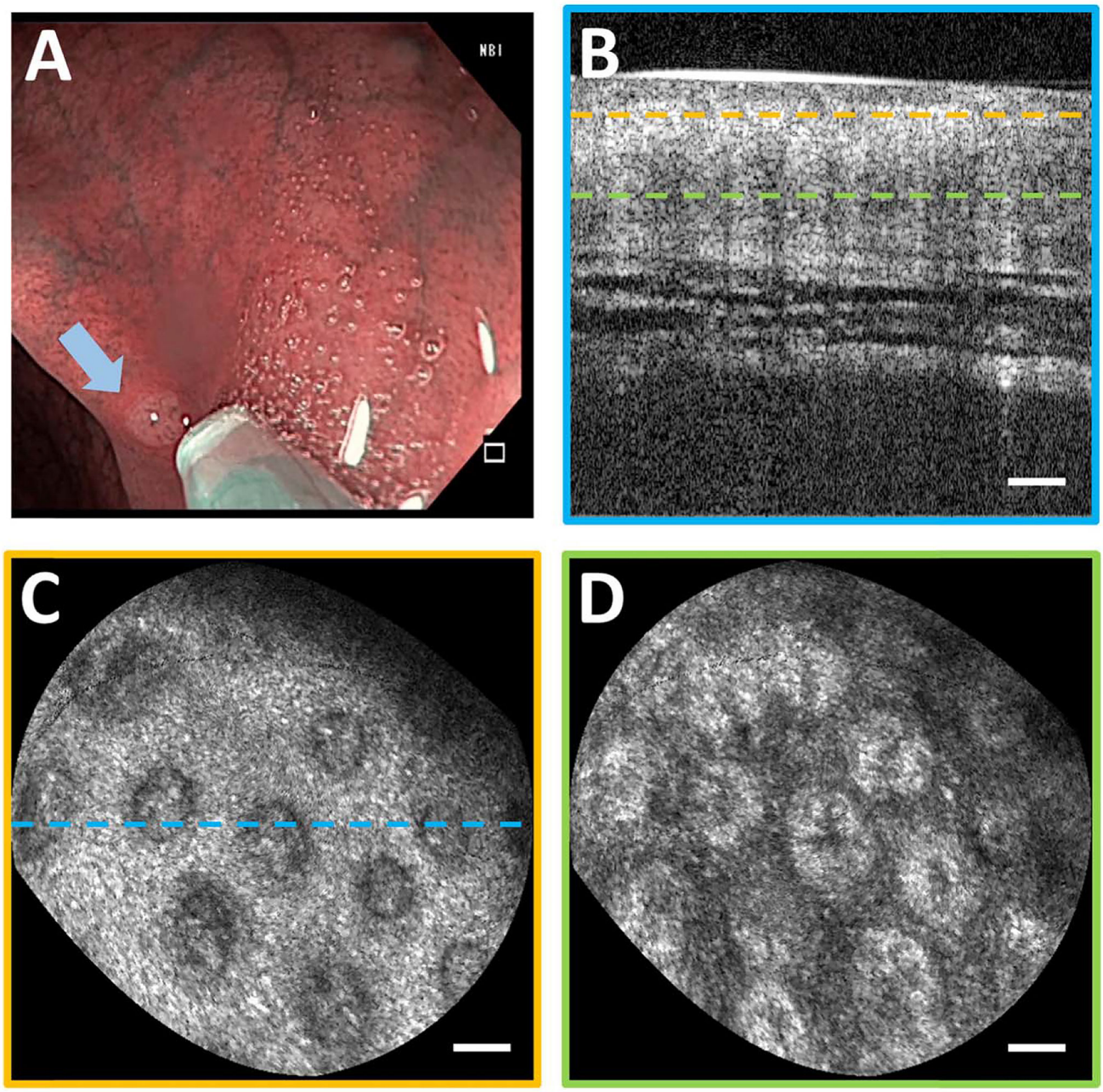

Fig. 4.

(A) Endoscopic image showing probe coming into contact with hyperplastic polyp (arrow). (B) Cross-section of OCT volume from polyp. *En face* OCT slices of 40 μm depth projection at (C) 40 μm depth and (D) 200 μm depth showing enlarged crypts. Scale bars 100 μm.

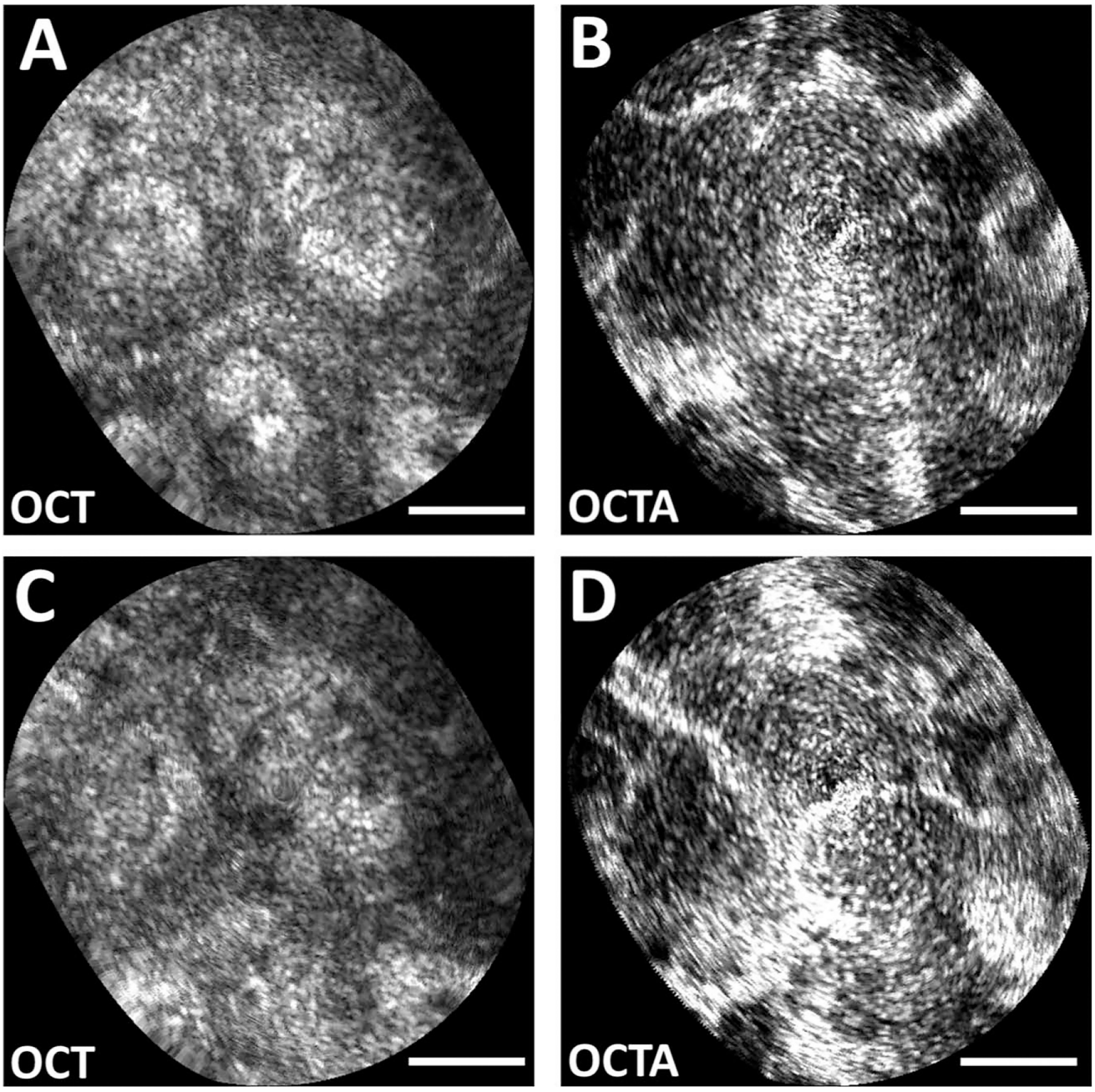

Fig. 5.

Zoomed *en face* OCT images at (A) 150 μm and (C) 200 μm depth (40 μm depth projection) of polyp. Intrinsically co-registered, depth-resolved OCT angiography from (B) 150 μm and (D) 200 μm depth showing vascular morphology. Scale bars 100 μm.